Solvo-thermal Assisted-Synthesis; Experimental and Theoretical Characterization; and Biological Evaluations of Azo-Chelator-Ligand Chelates of Fe(II) and Zn(II) ions

Festus Chioma [a*]

[a] *Department of Chemistry, Ignatius Ajuru University of Education, P.M.B. 5047, Rumuolumeni, Port Harcourt, Rivers State, Nigeria.*

Author's contribution

The sole author designed, analyzed, interpreted and prepared the manuscript.

Original Research Article

ABSTRACT

Background and Objectives: The resistance of microbes against anti-bacteriological drugs leading to countless deaths and terminal ailments remains a basis for concern. Hence, the main interest of this study was to design, synthesize and report unusual compounds with basic hydrophilic moieties plus hydrophobic functions for anti-bacteriological studies.
Materials and Methods: Analytical (melting points, micro-analysis (C. H.N.S) magnetic susceptibility (μ_{eff}), molar conductance plus solubility test) methods; spectral (Fourier Transform Infrared(FTIR)), electrospray ionization mass spectrometry (ESI-MS), nuclear magnetic resonance (^{1}H- plus ^{13}C-NMR), electronic(UV-Vis)) measurements; theoretical (DFT) evaluations were utilized for the characterization of the chelator and its chelates. All synthesized compounds were examined for antimicrobial and antioxidant potentials while the chelator was singly evaluated for solvent extractive capacity.
Results: A nitrogenous based chelator-ligand, (E)-1-(((4,6-dimethylpyrimidin-2-yl)imino)methyl) naphthalen-2-ol(LH) synthesized through reflux-condensation reaction of 2-amino-4,6-dimethylpyrimidine with 2-hydroxy-1-napthaldehyde was acquired. Further reflux of the chelator-

---

Corresponding author: Email: festchi@yahoo.com;

ligand with bivalent ions of iron-sulphate and zinc-acetate salts plus 2,2'-bipyridine resulted into separate bivalent-heteroleptic metallic chelates. The deprotonated nitrogen of the amine moiety and carbon of the carbonyl gave rise to the chelator-ligand with N_2O_2 chromophore detected around the metallic atom in the chelates. The μ_{eff} data plus UV-Vis spectral values of the chelates conformed to 6-coordinate octahedral geometry. All the chelates were high spin and non-ionic in dimethylsulfoxide (DMSO). The antimicrobial and antioxidant screening of the compounds presented moderate to fantastic results, while the metallic extractive proficiency of the chelator showed outstanding extractability for Fe^{2+} and Zn^{2+}ions with an efficiency of 79.34% and 51.92% correspondingly.

Conclusion: All the synthesized compounds are novel and demonstrated prospective biological, plus metallic ions' extractive potentials required for designs plus isolation of products also for such actions.

1. INTRODUCTION

Research undertakings on the improvement of metallic based antimicrobial drugs have had reasonable breakthroughs over the years. However, drug resilient bacteriological organisms has remained of utmost scientific concerns [1]. Countless metallic-based medications [2]. have been prepared as well as evaluated against manifold drug resisting microbes [3] like methicillin resistant *Staphylococcus aureus,* vancomycin resistant *E. faecium* and penicillin resistant *S. pneumoniae* strains [4], however, with only few making it to preclinical trials. The major challenge lies with the risk of metal poisoning due to high level of toxicity among metal based drugs [5]. Hence, the focus in the growth of more operative anti-bacteriological as well as anti-fungiform drugs is to synthesize drugs with broad spectrum antimicrobial potentials; of low toxicity, that can easily diffuse across microbial intracellular membrane, improved selectivity and with novel mechanisms of action [6].

The workability of anti-bacterial activities for most anti-bacteriological drugs remains a basis for their attraction [7] to the transpeptidase target enzyme within the bacteria, potential to permeate the bacterial cell membrane in addition to the grade of openness to β-lactamases emitted by certain microbial strains like *Klebsille pnemonie* for detoxification drugs [8,9]. For enhancement of the aforementioned potentials, our interest remains to design unusual compounds with basic hydrophilic moieties [7]; OH, NH, NH_2, CO_2H that stimulates lipophilicity of drugs via lipid cell membrane of countless microorganisms, as well as drugs having hydrophobic functions; C=N, -CH_2-, C=C which triggers sensitivity amid resistant Gram positive microbial strains [9].

Pyrimidine based compounds are acknowledged for excellent potentials in stabilizing biomolecules [10,11] that could be used as connectors in organic synthesis and good ligating ability in the formation of metal complexes [12]. Metallic chelates encompassing pyrimidinyl function group are known to demonstrate exceptional antimicrobial actions, a consequence of their interesting topologies, assemblage liability, selectivity to countless molecular environs, capability to display infrequent geometries unusual to resistant bacteria as well as their capacity to avert prompted oxidative stress damages [13]. This work reported the solvo-thermal assisted-synthesis new azo-chelator-ligand with its Fe(II) and Zn(II) chelates. The experimental and theoretical characterization in addition to the efficiency of the compounds as broad-spectrum *in vitro* antimicrobial agents were separately appraised

2. MATERIALS AND METHODS

2.1 Materials

The reagents/solvents adopted for this research without further purification were acquired from Merck o, Sigma-Aldrich o., and ACE Co. All the experimental works of this study were carried out at the research laboratory of the Department of Chemistry, Ignatius Ajuru University of Education, Rivers State, Nigeria form February-July, 2021.

2.2 Synthesis and Physical Measurements

The chelator-ligand, ((E)-1-(((4,6-dimethylpyrimidin-2-yl)imino)methyl)naphthalen-2-ol); and its metallic-chelates (aquo-(E)-(((l1-oxidaneyl)dioxo-l-6-sulfaneyl)oxy)((1-(((4,6-dimethylpyrimidin-2-yl)imino)methyl)naphthalen-

2-yl)oxy)iron and aquo-(E)-acetoxy((1-(((4,6-dimethylpyrimidin-2-yl)imino)methyl)naphthalen-2-yl)oxy)zinc) were synthesized following an already reported synthetic procedure [14] as presented in schemes 1 and 2 below. The uncorrected melting points via a digital melting point device were acquired, whereas molar conductance stood verified via Systronic Conductivity Bridge **304**. Synthesized compounds were evaluated by assessment of spectral (UV-Visible, NMR, ESI-MS, FT-IR); analytical and melting point values with comparable literature reports. The absorbance wavelength was obtained through on a Perkin Elmer Lambda 40 UV–Vis spectrometer with a quartz cuvette. The FT-IR spectra (50-4400 cm^{-1}) were acquired on a Bruker alpha-P FT-IR spectrometer adopting dehydrated KBr as reference. Microanalyses stood acquired via an Elementar Vario-EL-Cube set-up for CHNS evaluation. A Gouy magnetic balance was adopted for magnetic susceptibility determination of the metallic chelates at $27^{o}C$. The spectra of ^{1}H plus ^{13}C NMR in addition to Electrospray Ionization Mass Spectrometry were acquired on a Jeol 400 MHz spectrometer adopting deuterated $d6$-$(CH_3)_2SO$ as the solvent while tetramethylsilane (TMS) served as internal standard; and on a Waters Micromass Q-TOF II Mass Spectrophotometers separately

2.3 The Extraction Process

The extraction of the metallic species from the aqueous phase into organic phase (portion) using the recently synthesized chelator-ligand was examined via solvent extraction. 20 mL of aqueous solutions comprising 0.0017M of the metallic acetate salts remained equilibrated with equal volume of chloroform consisting of 0.00045M of the chelator-ligand by stirring forcefully at $27^{o}C$ on a motorized-shaker for 2-hrs.This was followed by careful transfer of the solution into a separatory funnel allowed to stand for ½-hr to establish equilibrium. The aqueous portion was then separated from the organic portion with concentration of metallic ions determined in both phases via atomic adsorption spectrophotometer (AAS). The extraction efficiency, E (%) was acquired according to Eq. 1 [15].

$$E\ (\%) = \frac{D}{D + \frac{A}{O}} \times 100 \qquad (1)$$

The solvent extraction procedures could be described by Eq. 2 in which metallic ion (M^{n+})

forms a chelate with the chelator-ligand (LH) to afford a neutral structural assemblage (ML_x).

$$M^{n+}\ (aq) + xHL(org) \rightleftharpoons ML_x\ (org) + nH^{+}(aq) \qquad (2)$$

The mechanism of extraction correlates with a cation interchange where a complex of stoichiometric formula ML_x is established in the organic phase producing n mol of H^{+} in the aqueous phase. Hence, the extraction constant (K_{ext}) can be stated as;

$$K_{ext} = \frac{[ML_x]_{(org)}\ [H^{+}]^{n}_{(aq)}}{[M^{n+}]_{(aq)}\ [HL]^{x}_{(org)}} \qquad (3)$$

Since the metallic ion M^{n+} is predominant in the aqueous phase and ML_x is the only extractable specie, the distribution ratio, D can be calculated following Eq. 4. The D is used as the most imperative index for determining the adeptness of a solvent extraction procedure.

$$D = \frac{[ML_x]_{(org)}}{[M^{n+}]_{(aq)}} = \frac{Metal\ ions\ concentration\ in\ the\ organic\ portion}{Metal\ ions\ concentration\ in\ the\ aqueous\ portion} \qquad (4)$$

2.4 Biological Studies

Anti-bactericidal evaluation of the Fe(II) and Zn(II) chelates alongside their chelator-ligand were obtained via an agar well diffusion technique [16] with DMSO as reaction medium. The bacteria strains, reference drugs and procedural steps reported in our previous study [17]. were adopted with the sole aim of finding the most active compound with the best antibacterial potentials.

A disc evaluative practice was adopted in-vitro to appraise the anti-fungoid actions of the chelator-ligand and its metal-chelates against *A. niger, A. flevus* and *R. Stolonifer*. Potato dextrose agar (PDA) served as medium for the harvest of matured conidia of fungal isolates which were suspended in ringer solution. A 1 mL conidial suspension for a separate fungoid isolate was inoculated on a petri dish of 90 mm with 20 mL PDA. The chelates with the chelator in DMSO were dissolved (10 mg/mL, 5 mg/mL and 1 mg/mL). Bored germ-free 7mm diameter disc holes were filled (0.15 □L) with individual test compound's solution and experimental data acquired in duplicate at three altered concentrations. Fluconazole as adopted as reference drug while DMSO stood as the negative control. The inhibition growth zones were evaluated after 24 h and expressed as the inhibition zone in mm.

2.5 Quantum Chemical Calculation (QCC)

The chelator for appraisal remained evaluated via DFT, adopting Becke's 3-parameter hybrid interchange function fused to Lee-Yang-Parr correlation functional (B3LYP) by means of 6-311G++(d,p) simple set. All QCCs stood completed adopting Gaussian-9-package. Optimized structural geometry as well as visualization into HOMO plus LUMO calculations remained acquired via gauss-View 5.0.8 package enabling the determination of other parameters. With Molinspiration cheminformatic, all pharmacokinetic factors stood acquired for prediction of bioactivities of the chelator though the property explorer appraisal afforded relevant data on the relative cytotoxicity of the chelator.

3. RESULTS AND DISCUSSION

3.1 Synthesis and Preliminary Investigational Data

The synthesized chelates with their chelator-ligand exhibited various shades of colour (Table 1). The $[Fe(L)(B)(SO_4)].H_2O$ and $[Zn(L)(B)(OAc)].H_2O$ chelates displayed shades of brown and yellow separately, while the HL adopted a bright yellow shade. Distinct and sharp melting points different from that of the starting materials were generally obtained for all synthesized compounds (Table 1). Excellent correlations were observed amid acquired experimental and calculated values for percentage metallic ratios determined through complexometric titration method as presented in table 1. The molar conductance values (Table 1) of the chelates obtained in dimethylsulphoxide (DMSO) were between 9.7–12.0 $Ohm^{-1}mol^{-1}cm^2$ indicative of non-ionic status for the soluble chelates. The latter arises from literature reports which affirms that values of 45-90 $Ohm^{-1}mol^{-1}cm^2$ and 90-120 $Ohm^{-1}mol^{-1}cm^2$ are generally for 1:1 and 1:2 ionic chelates. The molar conductance data remained intensely validated by the micro (CHNS) plus quantitative analyses data in which no anions were noticed. The solubility tests of the chelator and its chelates obtained in polar and non-polar organic solvents gave varied solubilities (Table 2). The compounds were majorly or slightly insoluble in H_2O, CH_2Cl_2 and CH_3NO_2. Moreover, the compounds had good solubilities in chloroform, dimethylsulfoxide and dimethylformamide but were sparingly soluble in ethanol, methanol and dichloromethane. The chelator and chelates had moderate-good (46-59%) yields (Table 1). The micro analysis, C, H, N, S data for the chelator and its chelates shown in table 1 have been obtained and the values remains consistent with the theoretical values corroborating 1:1:1 stiochiometries for the heteroleptic chelates and conforms with the empirical formula suggested for each compound

3.2 Extraction of Metallic Ions Using the Synthesized Chelator-Ligand

The extraction proficiencies of the chelator-ligand were evaluated by means of solvent extraction on d^6 and d^{10} metallic ions (Fe^{2+} and Zn^{2+}) into chloroform under neutral conditions. The table 3 below illustrated the number of metallic ions in the aqueous as well as organic phases after the extraction in addition to the extractability of the chelator-ligand.

From the extraction data presented in table 3, it was noticed that the chelator displayed high extractability for Fe^{2+} with extraction efficiency of 79.34%, and showed a fair extractability potential for Zn^{2+} with extraction efficiencies of 51.92%. The chelator-ligand exhibited moderately good extractability for the metallic ions.
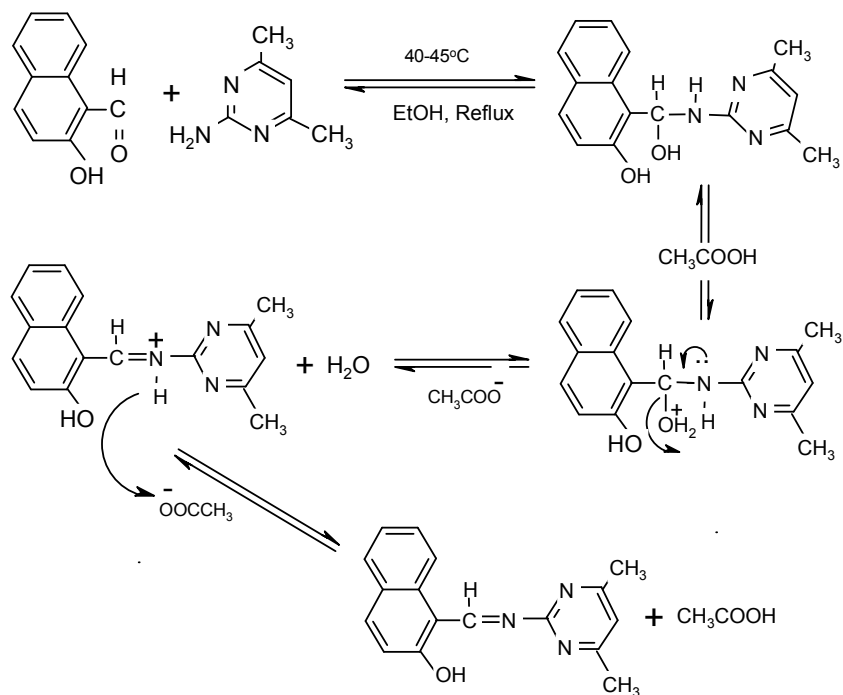
3.3 NMR Studies

The ^1H-NMR spectrum of the chelator-ligand was shown Fig. 4 and its signal positions presented in table 4a. The methyl protons on the pyrimidine ring gave sharp singlet peak around 3.34 ppm while the C_5 proton resonated around 6.65 ppm. Equally, the protons (H_{15}, H_{16}, H_{17} and H_{18}) of the napthalene ring appeared as twofold-signals around 7.83-7.84, 7.10-7.29, 7.50-7.53 as well as 7.64-7.66 ppm in addition to lone-signals (H_{11} and H_{12}) around 8.03 ppm plus 7.31 ppm separately. The signals around 14.42 ppm plus 9.55 ppm were corroborated the phenolic proton plus C=N proton in the chelator-ligand spectrum. The latter validates the existence of OH as well as formation of the chelator. The $^{13}CNMR$ spectrum (Fig. 5) displayed resonance signals (Table 4b) characteristic of napthalene C_{11}-C_{20} atoms at 108.06, 133.7, 129.2, 129.5, 126.3, 124.5 ppm and 119.3 ppm singly. The signal at 141.3 remained consistent of the azomethine C-atom (C_{10}), while detected signals around 183.8 ppm, 168.7 ppm as well as 116.8 ppm remained separately ascribed to C_2, $C_{4,6}$ plus C_5 atoms of the pyrimidine function. Consequently, $C_{7,8}$ appeared as lone signal around 23.44 ppm.
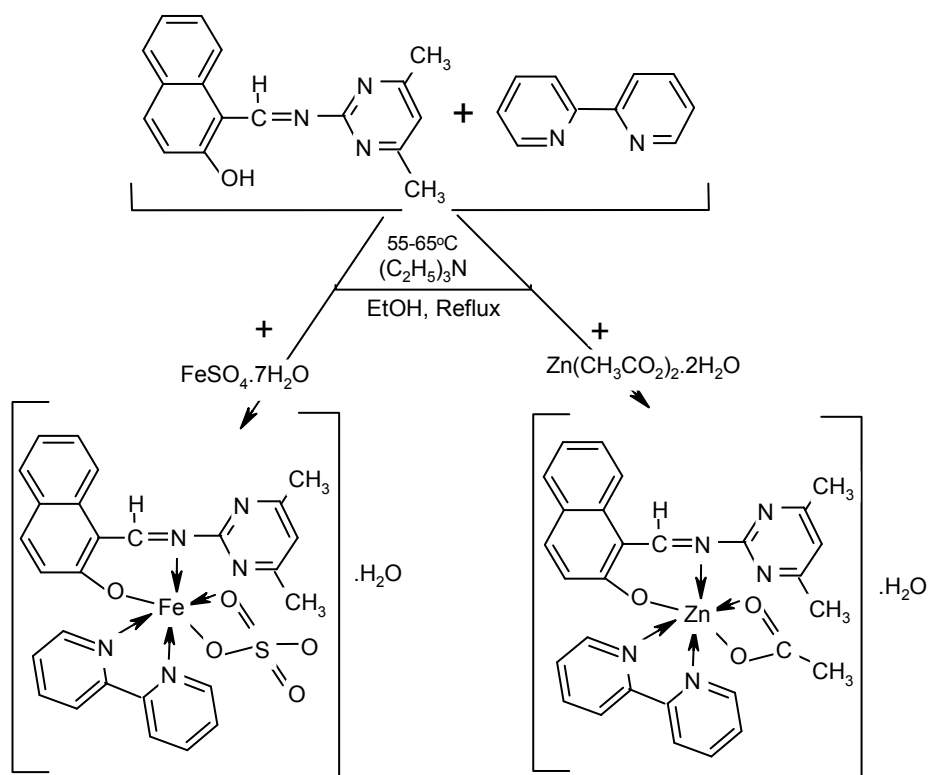
Table 1. Analytical data for HL Chelator-ligand plus its heteroleptic Fe(II) and Zn(II) Chelates

Molecular Formula	Formula Weight (g/mol)	Colour	Melting Point (^{o}C)	Yeild (%)	μ_{eff} (B.M)	Molar Conductance (Ohm^{-1}Mol^{-1}cm^2)	Analytical/Found (Calculated) %				
							C	H	N	S	M
HL $C_{17}H_{15}N_3O$	278.86	Yellow	194-196	59.30	-	-	73.94 (73.89)	5.53 (5.47)	15.41 (15.23)	- -	- -
B	156.18	White	63-66	-	-	-	-	-	-	-	-
[Fe(L)(B)(SO$_4$)].H$_2$O [FeC$_{27}$H$_{22}$N$_5$O$_5$S].H$_2$O	602.368	Redish Brown	319-321	46.00	4.97	12.08	53.99 (53.83)	4. 05 (4.02)	11.68 (11.63)	5.52 (5.32)	9.56 (9.27)
[Zn(L)(B)(OAc)].H$_2$O [ZnC$_{29}$H$_{25}$N$_5$O$_3$].H$_2$O	574.676	Bright Yellow	289-291	51.30	0.24	9.71	60.64 (60.60)	4.83 (4.74)	12.22 (12.19)	- -	11.44 (11.38)

Key: B = 2,2'-Bipyridine; SO$_4$ = Sulphate; OAc = Acetate; μ_{eff} = Effective Magnetic Moment Value; B.M = Bohr Magneton

Scheme 1. Synthetic Procedure for the Chelator-Ligand

Scheme 2. Synthetic Diagram and Proposed Structure for the Metallic Chelates

Table 2. Solubility results of HL Chelator-ligand and its heteroleptic M(II) Chelates

Compound	Distilled H_2O	MeOH	EtOH	CH_2Cl_2	$CHCl_3$	DMSO	DMF	CH_3NO_2
HL	SS	SS	S	SS	S	S	S	SS
$[Fe(L)(B)(SO_4)].H_2O$	SS	S	S	SS	S	S	SS	SS
$[Zn(L)(B)(OAc)].H_2O$	SS	SS	SS	SS	SS	SS	SS	SS

Key: S=Soluble; SS=Slightly Soluble; NS=Not Soluble

Table 3. Extraction Efficiency of HL Chelator-Ligand

Metallic ion	Aqueous phase (mg/L)	Organic phase (mg/L)	Distribution ratio	Percentage extraction (%)
Fe^{2+}	0.8201	3.1454	3.84	79.34
Zn^{2+}	0.0682	0.0734	1.08	51.92

Table 4a. ^{1}Hnmr data of the synthesized Chelator-ligand, HL in ppm

Chelator	$C_{10}H_6$	C_4H_6-N_2	$C_{10}H_4$-O_2	HC=N	O-H	CH_3	N-H
HL $C_{17}H_{15}N_3O$	7.10-7.84	6.65	-	9.55	14.42	3.34	-

Table 4b. ^{13}Cnmr data of the synthesized Chelator-ligand, HL

Chelator	$C_{10}H_6$/C_8H_5	C_4H_6-N_2	$[-C=O (-one)]_2$	HC=N	CH_3
HL $C_{17}H_{15}N_3O$	108.06-133.7	116.8-183.8	-	141.3	23.44

Table 5. Infrared spectral (cm^{-1}) data of the Chelator-ligand with its heteroleptic Chelates

Compounds	v(OH)	v(C=N)	v(C=C)	v(C-N)	v(C-C)	v(C-O)	δC-H	M-N	M-O
HL	3441$_b$	1628$_s$	1593$_s$	1537$_s$	1432$_s$	1290$_s$	981$_s$	-	-
B	-	1639$_s$	1580$_s$	1453$_s$	1349$_s$	-	991$_s$	-	-
$[Fe(L)(B)(SO_4)].H_2O$	3439$_b$	1614$_s$	1574$_s$	1529$_s$	1345$_m$	1185$_m$	985$_s$	547$_m$	451$_m$
$[Zn(L)(B)(OAc)].H_2O$	3434$_b$	1619$_s$	1589$_m$	1532$_s$	1334$_m$	1188$_s$	835$_m$	594$_m$	452$_m$

Key: b = broad, s = sharp, d = doublet and m = medium

3.4 FT-IR Data

The FT-IR spectrum of the chelator-ligand presented no bands arising from amino groups as noticed within the spectrum of the precursor amine adopted for synthesis indicative of condensation via the amino group with the aldehyde [18]. Acquired spectral bands necessary for structural estimations for the synthesized compounds are presented in Table 5. The broad to medium band centered at 3440 cm^{-1} remained apportioned to intra-proton-bonding vibrations (vO-H....N) of an enol assemblage frequently detected in chelators consisting of terminal OH functions. The band remained absent in the spectra of the chelates validating chelation via the naphthol oxygen atom of the chelator. Though, observed medium-broad bands from 3348 cm^{-1} - 3447 cm^{-1} in the spectra of metallic chelates remained attributed to vOH of hydrated H_2O molecules [11]. While the sharp-medium H-stretching bands of the aromatic rings, v(Ar–H), within the chelator appeared amid 3013-3001 cm^{-1}, the chelates displayed medium asymmetric plus symmetric stretching vibrations for the alkyl groups within 2929-2913 cm^{-1}. The absorption band at 1628 cm^{-1} due to C=N moiety moved to lower/higher frequencies in the chelates to the range 1614-1667 cm^{-1}, substantiating participation of the azomethine N in chelation with the M(II) ions [12]. The new band, C=N in addition to the cyclic C=C vibrations almost appeared at equal strength in the chelator from 1628 cm^{-1} to 1593 cm^{-1} but were observed at lower/higher frequencies by ± 30cm^{-1} in the chelates. The C=N function was

apportioned to participation of the imine *N* in interaction with the M(II) ions, while the C=C was a consequence of aromatic conjugations plus the effect of chelation [19,20]. The status of *v*(C=N) remained same (single) in the spectra of all compounds suggestive of Fermi resonance [12,21]. On the other hand, the band around 1290 cm^{-1} within the chelator's spectrum was accredited to *v*(C-O) which displayed significant shifts to greater/lesser frequencies in the spectra of the chelates owing to chelation. The sharp band in the spectrum of the chelator observed at 981 cm^{-1} was due to *δ*CH. The *δ*CH band still appeared prominent in the chelates nonetheless moved to greater wavenumbers (977-830 cm^{-1}). The M-N and M-O bands were detected around 594-547 as well as 452-451 cm^{-1} separately, confirming chelation via the imine *N* and enol *O* atoms.

3.5 UV-VIS and Magnetic Susceptibility Studies

The UV-Vis spectra of the chelates with their chelator (Table 6) were acquired [7,22] amid 19000-90000 cm^{-1}. Absorption signals remains the outcome of transitions of electrons within the chelator's molecular orbitals (n→π*, π→π*), metallic *d-d* transitions as well as charge transfer (CT) transitions (M→L plus L→M CT) [22]. The absorption signals centered at 29019 cm^{-1} within the chelator's spectrum exhibited significant shifts in the chelates conforming to n→π∗ transition of the C=N functions. Also, the transition π→π∗ of the chelator observed at 32362 cm^{-1} remained almost unaltered in the spectra of the chelates. The signals amid 26607-44052 cm^{-1} in the iron chelate were characteristic of π*←n, π*←π plus CT transitions. The visible

signals at 22727 cm^{-1} (140 L cm^{-1} mol^{-1}) and 18904 cm^{-1} (170 L cm^{-1} mol^{-1}) remain *d-d* signals apportioned to UV-Vis transitions of $^5T_{2g} \rightarrow {}^5A_{1g}$, and $^5T_{2g} \rightarrow {}^5B_{1g}$ separately characteristic of an bivalent iron chelate with octahedral geometry [23-25]. The synthesized iron chelate exhibited magnetic moment at 4.97 B.M. consistent with assigned geometry [26]. The spectrum of the bivalent zinc chelate expectedly presented CT transitions (M→L) at 13123 cm^{-1} and 23419 cm^{-1} as no *d-d* transition was anticipated for d^{10} zinc chelates [27]. The signals at 26290 cm^{-1} and 31949 cm^{-1} were typical of intra-chelator signals. Bivalent zinc chelates holds $3d^{10}$ electron arrangement besides displays magnetic moments of almost zero unpaired electrons. Acquired *μ*$_{eff}$ of 0.24 B.M. denotes diamagnetism for the Zn(II) chelate as well as validates its geometry [28,27].

3.6 The ESI-MS Studies

The ESI-mass spectrum (Fig. 6) of the chelator-ligand presented dual pathways of disintegration with a base peak m/e+ at 278.12 conforming to the estimated molecular weight (278.85) for the chelator-ligand (Table 7). This substantiates the formation of form HL chelator from 2-hydroxy-1-napthaldehyde plus 2-amino-4,6-dimethylpyrimdine. The signals at m/z 250.17, 193.66 plus 142.92 were arising from loss of COH, NC$_2$H$_2$O and C$_2$N$_2$H components while the peak at m/z 124.81 remained undoubtedly due to OH lost separately. Additionally, the spectrum had L+1 peak at m/z 279.24, a small strength peak at m/z 280.11 which can be ascribed to additional mass units, a result of C-13 existence as well as extra average peak around 276.12 owing to lose of protons

Table 6. Electronic spectra data for the Chelator-ligand plus its heteroleptic M(II) Chelates

Compounds	Absorption Bands (cm^{-1})	Bands Assignment	Tentative Geometry
HL	32362	π − π*	-
	29019	n − π*	
[Fe(L)(B)(SO$_4$)].H$_2$O	44052	C.T	Octahedral
	39682, 30769	π − π*	
	26607	n − π*	
	22727	$^5T_{2g} \rightarrow {}^5A_{1g}$	
	18904	$^5T_{2g} \rightarrow {}^5B_{1g}$	
[Zn(L)(B)(OAc)].H$_2$O	31949	π→π*	Octahedral
	26290	n→π*	
	23419	M→L	

Table 7. Mass spectra result for the Chelator-ligand

Ligands	Fragmentation	
	m/e	m/z
HL		279.24 [m+1], 280.11 [m+2]
$C_{17}H_{15}N_3O$	278.12	276.12 [$-H_2$, 2.016], 250.17[COH]$^+$, 193.66[NC$_2$H$_2$O]$^+$,
[278.86]		142.92[C$_2$N$_2$H]$^+$, 125[OH]$^+$

Keys: EMU=Extra mass unit

3.7 Biological Evaluations

Acquired antibacterial studies data are accessible in Table 8 below. From the table, it is obvious that the heteroleptic Fe(II) and Zn(II) chelates were largely sensitive with varying degrees of inhibitory impacts on the growth of the screened organisms compared to the ligands ('L and B'); a consequence of chelation [13,14]. Also as observed from the data, the enhanced sensitivity of the chelates with their chelator against the gram positive stains than the gram negative microbes is explainable on the basis of differences in the cell-wall compositions of the microbes as well as the alteration in the penetrability plus permeation of the compounds through the microbial cell membranes [22]. The over-all inhibition of the microbes by the chelator with inhibitory zones of 12.0-19.0 mm could be attributable to the presence of π-electrons within the cyclic moieties as well as the C=N functions frequently acknowledged to improve antibacterial actions [29,30] heterocyclic assemblages. The

Fe(II) chelate demonstrated inhibitory growth effect better than that of the chelators ('L' and 'B') against only *B. cereus* (19.5 mm) and *S.aureus* (21.0 mm) indicating its potential significance in new antibacterial drug designs. Though the Zn(II) chelate remained moderate in its actions against the tested microbes. The latter may be assigned to creation of persuasive protein poisons within the cell-surfaces of the microbes averting further penetration of the Zn(II) chelate into the inner portions of the microbial cells as well as imposing lessened lipophilicity of same chelate which automatically reduces permeation into the lipid cell membrane of the microbes [20,31]. The antifungal activities of HL chelator-ligand and its asymmetrical metallic chelates against *A. niger, A. flevus* and *R. Stolonifer* are contained in Table 9. The chelator-ligand had activity against all the tested species except *R. Stolonifer* which showed resistance. The Fe(II) and Zn(II) chelates were suggestively active against *A. flevus* and *A. niger* only with inhibitory zones of 15.0 - 21.0 mm.

Table 8. Antibacterial data of HL Chelator-ligand and its heteroleptic M(II) Chelates

Compound/Bacteria	A	B	C	D	E	F
HL	17.5±2.1	17.0±2.8	15.0±0.0	12.0±2.8	19.0±1.4	14.0±2.8
B	15.5 ± 0.7	12.0 ± 2.8	26.0 ± 2.8	8.5 ± 0.7	17.0 ± 4.2	19.5 ± 2.1
[Fe(L)(B)(SO$_4$)].H$_2$O	19.5±3.5	15.5±0.7	18.0±1.4	9.0±1.4	21.0±2.8	18.5±2.1
[Zn(L)(B)(OAc)].H$_2$O	16.0±0.7	14.0±2.8	8.5±0.7	12.0±1.4	14.5±0.7	13.5±0.7
$^+$Ciprofloxacin	33.0 ± 3.5	32.0 ± 1.4	36.0 ± 2.8	26.5 ± 0.7	29.0 ± 2.1	23.0 ± 1.4
-DMSO	0.0±0.0	0.0±0.0	0.0±0.0	0.0±0.0	0.0±0.0	0.0±0.0

Key: A= B. cereus; B = E. coli; C = K. oxytoca; D = P. aeruginosa; E = S.aureus; F= P. mirabilis

Table 9. Antifungal result for the Chelator-ligand and its M(II) Chelates

Fungal/Compounds	G	H	I
HL	19±1.4	21±0.7	-
B	16±1.6	19±1.4	13±0.7
[Fe(L)(B)(SO$_4$)].H$_2$O	15±1.4	17±0.0	-
[Zn(L)(B)(OAc)].H$_2$O	17±2.1	21±0.0	-
$^+$ Fluconazole	36±0.3	29±0.7	38±0.3
-DMSO	-	-	-

Key: G = A. niger; H = A. flevus; I = R. Stolonifer

3.8 Antioxidant Studies

The chelator-ligand with its M^{2+} chelates were appraised for radical scavenging actions using DPPH (1,1-diphenyl-2-picryl-hydrazyl) radical at 200, 100 plus 50 $\mu g/mL$ concentrations in 1mL DMSO. Acquired data on the basis of percentage inhibition are obtainable in Table 10. A good analysis of the data designates that the chelator plus its chelates largely demonstrated radical scavenging actions in DPPH assay. Inhibitory values commonly reflect degree of radical scavenging actions. The chelator-ligand substantively exhibited percentage inhibitory values smaller or comparable to that of standard suggestive of its anti-oxidant abilities. The potentials of the chelator-ligand got enhanced noticeably on chelation with M(II) ions. Largely, the metallic chelates presented superior DPPH radical scavenging actions.

Subsequently, the data of the DPPH antioxidant actions attested that the compounds could be adopted for design as well as syntheses of drugs for the management of pathological illnesses rising from oxidative stress.

3.9 Quantum Chemical Studies

The Frontier Molecular orbital allows for the prediction of reactivity of the chelator whose active site could be established by the distribution of the orbital frontiers. The HOMO is seen as a nucleophile, while LUMO. The LUMO is seen as an electrophile which accepts electrons from nucleophile. Several chemical reactivity descriptors, such as the chemical potential, global hardness and electrophilicity, have been calculated and is presented in Table 11.

Table 10. Antioxidant Data for the Chelator-ligand and its heteroleptic Fe(II) and Zn(II) Chelates

Compounds	Concentration	Absorbance			Mean (Error)	% Inhibition (Error)
		1	2	3		
Blank	-	0.77	0.78	0.78	-	-
HL	Ic_{50}	0.09	0.09	0.09	0.58(±0.001)	86.56(±0.07)
	Ic_{100}	0.088	0.083	0.083	0.585(±0.003)	87.33(±0.46)
	Ic_{200}	0.082	0.078	0.079	0.590(±0.002)	88.1(±0.36)
B	Ic_{50}	0.172	0.170	0.168	0.501(±0.004)	74.76(±0.570)
	Ic_{100}	0.160	0.160	0.158	0.510(±0.002)	76.23(±0.234)
	Ic_{200}	0.152	0.152	0.150	0.518(±0.002)	77.40(±0.173)
$[Fe(L)(B)(SO_4)].H_2O$	Ic_{50}	0.167	0.167	0.168	0.502(±0.001)	75.03(±0.07)
	Ic_{100}	0.092	0.092	0.092	0.578(±0.001)	86.26(±0.07)
	Ic_{200}	0.050	0.057	0.050	0.617(±0.004)	92.16(±0.57)
$[Zn(L)(B)(OAc)].H_2O$	Ic_{50}	0.024	0.018	0.019	0.649(±0.004)	96.96(±0.49)
	Ic_{100}	0.005	0.011	0.014	0.66(±0.003)	98.53(±0.71)
	Ic_{200}	0.006	0.004	0.002	0.666(±0.003)	99.4(±0.30)
Standard Ascorbic Acid	Ic_{50}	0.093	0.089	0.094	0.578(±0.002)	86.26(±0.38)
	Ic_{100}	0.085	0.081	0.082	0.587(±0.002)	87.66(±0.32)
	Ic_{200}	0.078	0.074	0.076	0.594(±0.002)	88.67(±0.35)

Table 11. Quantum chemical parameters of Chelator-Ligand, HL

PARAMETER	
Energy (ev)	-24255.97417444094
E- lumo	-1.7179
E- homo	-5.9163
Energy gap	4.1984
Dipole moment (Debye)	3.4824
Ionization potential	5.9163
Electron affinity	1.7179
Electronegativity	3.8171
Hardness	2.0992
Softness	0.2382
Electrophilicity	3.4703

The global reactivity and local descriptors remained evaluated via Koopman's theorem equations expressed as:

Ionization potential (I) = -E-homo
Electron affinity (A) = -E-Lumo
Electronegativity (χ) = (I +A)/2
Hardness (η) = (I – A)/2
Softness (S) = 1/2 η
Electrophipilicity (ω) = $\mu2/2\eta$
where μ which is chemical potential is - χ

Low energy gap value denotes high chemical reactivity [32], while high energy gap signifies low chemical reactivity. The energy gap of the chelator was observed to be low which suggested high chemical reactivity. The electrophilicity is a measure in stabilization of energy when a compound accepts an extra electronic charge within its environ. Often perceived an improved descriptor of general chemical reactivity consisting of together the capacity of an electron-loving specie to obtain an extra electronic charge as well as the non-acceptance of a compound to undergo an electronic charge interchange in its environ. It offers basic facts on electron transfer (chemical potential) and stability (hardness). The 'χ' ascertains the attraction of electrons to an atom within a covalent bond. When two dissimilar atoms are bonded covalently, the shared electrons will be more strongly pulled towards the more electronegative atom [33]. The optimized, HOMO in addition to LUMO orbitals of our synthesized chelator are given below as Figs. 1-3 separately.
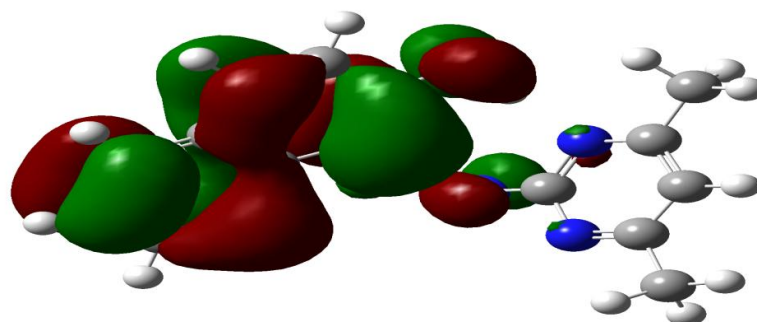

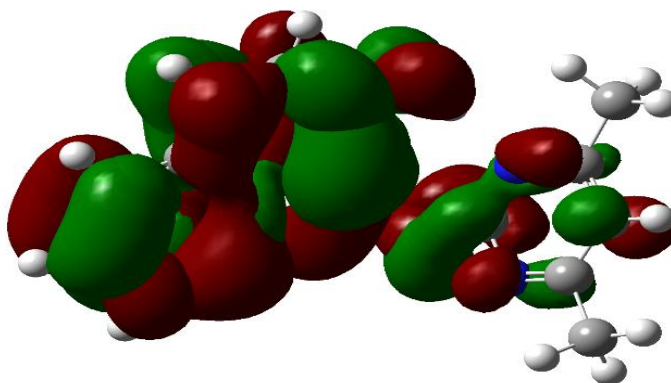**Fig. 1. Optimized Structure of HL Chelator**

Fig. 2. HOMO of HL Chelator

Fig. 3. LUMO of HL Chelator

The result as presented in Table 12 showed that the chelator's pharmokinetic parameters where within the Lipinski rule of five. This entails that the chelator will be of good oral bioavailability. A bioactivity score of more than 0 signifies a chelator's activeness. Between -0.5–0, it is moderately active and a value less than -0.5 suggests inactiveness. Table 13 shows the bioactivity scores of the chelator. Except for its enzyme inhibitor and Kinase inhibitor probability scores which fell within the moderately active zone. The chelator showed values that suggests inactivity for the remaining drug-likeness parameters. The risks of toxicity (mutagenicity, tumorigenicity, irritation, reproduction) as well as the physicochemical features (miLogP, solubility, drug likeness plus drug score) remained evaluated via a procedure established by property explorers and illustrated in Table 14. The cLogp and the solubility were observed to be within the acceptable criteria. , which suggested good absorption and distribution [33].

Table 12. Molecular Properties Descriptors

PHARMOKINETIC PARAMETERS							
Vol	TPSA	Nrotb	HBA	HBD	LogP	MW	Violation
-	-	-	< 10	< 5	≤ 5	< 500	≤ 1
255.33	58.38	2	4	1	3.63	277.33	0

Vol. volume; TPSA. Topological polar surface area; NROTB. number of rotatable bonds; HBA. number of hydrogen bond acceptors; HBD. number of hydrogen bond donors Log P. logarithm of compound partition; MW. molecular weight

Table 13. Bioactivity Score according to Molinspiration Cheminformatics Software

DRUG-LIKENESS					
GPCR	ICM	KI	NRL	PI	EI
-0.53	-0.75	-0.42	-0.52	-0.66	-0.26

GPCR ligand. ICM: Ion channel modulator, KI: Kinase inhibitor, NRL: Nuclear receptor ligand, PI: Protease inhibitor, EI: Enzyme inhibitor

Table 14. Property Explorer properties of the Chelator-Ligand

TOXICITY RISKS				PROPERTY EXPLORER CALCULATIONS			
MUT	TUM	IRRI	RE	cLogp	S	DL	DS
HR	HR	LR	LR	3.48	-0.47	-3.58	0.13

HR ; High Risk, LR; Low Risk,MUT : mutagenic ; TUMO : tumorigenic ; IRRI: irritant ; RE: reproductive effective ; CLP: cLogP ; S: Solubility ; DL : Drug-likeness ;DS : Drug-Score
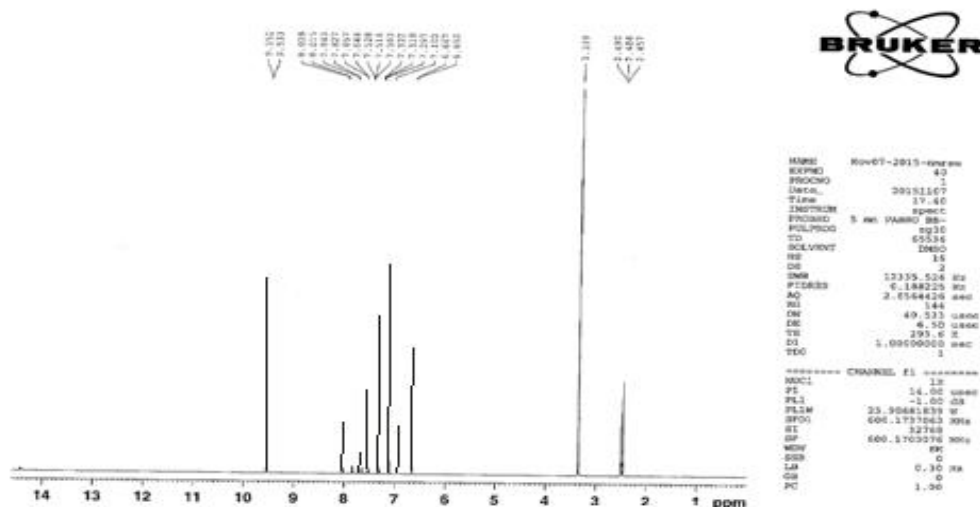

Fig. 4. ^{1}Hnmr spectrum of the Chelator-ligand

4. CONCLUSION

The N$_2$O$_2$ chelator-ligand with its bivalent heteroleptic Fe and Zn chelates were obtained through reflux-condensation reaction. Spectral plus analytical techniques were utilized for the characterization of the synthesized compounds. The deprotonated nitrogen of the amine moiety and carbon of the carbonyl reagent gave rise to the chelator-ligand with N$_2$O$_2$ chromophore

detected around the metallic atom of the chelates. The μ_{eff} data plus UV-Vis spectral values of the chelates conformed to 6-coordinate octahedral geometry and assigned same. The Fe^{2+} chelate displayed high spin whereas the Zn^{2+} chelate assumed spin-free configuration, however both chelates were non-ionic in dimethylsulfoxide (DMSO). The antimicrobial screening of the chelates presented moderate to excellent results but with respect to standard drug used, the tested compounds were found to be moderately active. The bivalent heteroleptic chelates demonstrated good scavenging actions like the standard drug adopted. The chelator-ligand was further evaluated for metallic extractive proficiency and an outstanding

extractability for Fe^{2+} and Zn^{2+}ions with an efficiency of 79.34% and 51.92% was acquired correspondingly.

SIGNIFICANT STATEMENT

Reflux-chelative process was unraveled in this study as a synthetic method for an N_2O_2 chelator-ligand with an enol tautomeric assemblage. Principally, the study established that the chelates demonstrated outstanding biological actions over their chelator against tested microbial organisms. However, the metallic ions' extractive potentials of the chelator-ligand as observed remained prospective
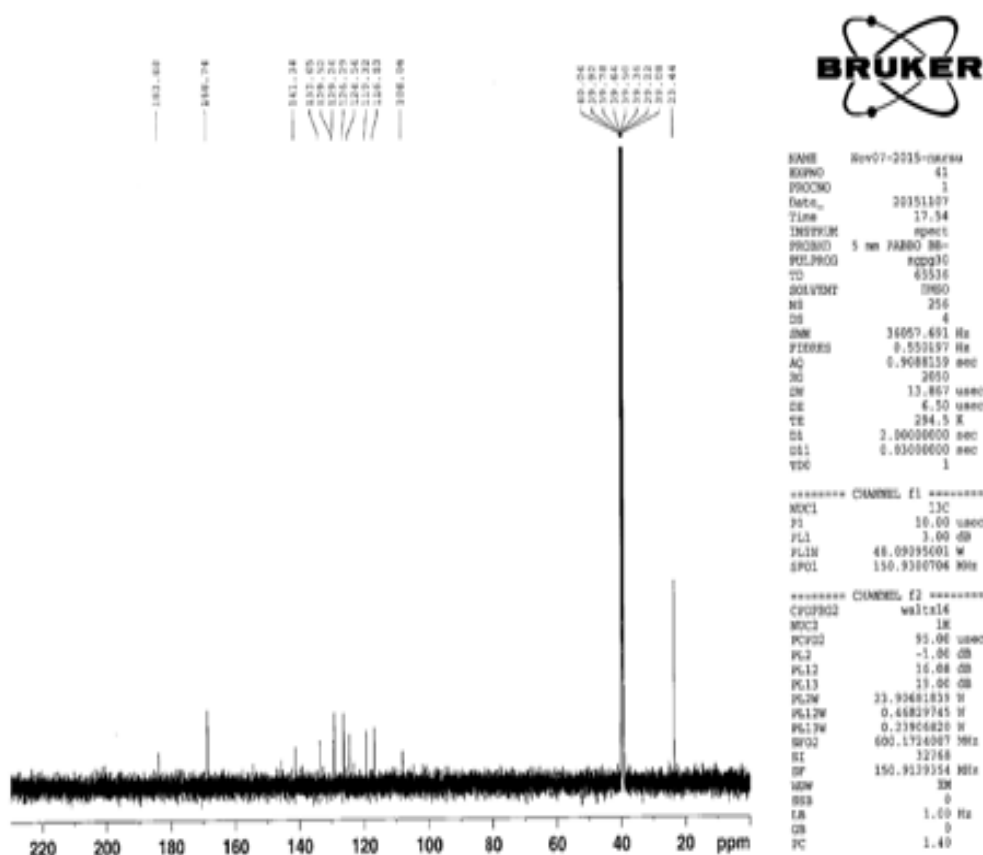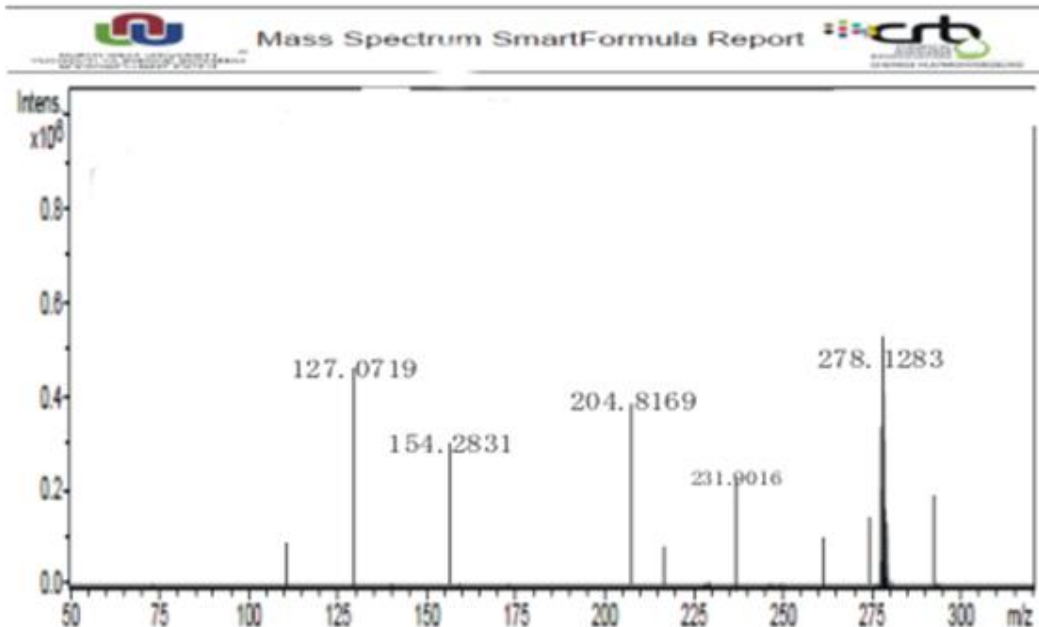

Fig. 5. ^{13}Cnmr spectrum of the Chelator-ligand

Fig. 6. Mass spectrum of the Chelator-ligand

COMPETING INTERESTS

Author has declared that no competing interests exist.

REFERENCES

1. Ekennia AC, Onwudiwe DC, Osowole AA. Spectral, thermal stability and antibacterial studies of copper, nickel and cobalt complexes of N-methyl-N-phenyl dithiocarbamate. J. of Sulfur Chem. 2014; 36(1):96-104.
DOI.org/10.1080/17415993.2014.969731
2. Patrick GL. An introduction to medicinal chemistry. 3rd Edn, Oxford University Press, UK; 2015.
3. Mc Quitty RJ. Metal-based drugs. Sci Prog. 2014;97(1):1-19.
DOI:10.3184/003685014X1389898018507 6.
PMID: 24800466
4. Richard JF, Yitzhak T. Antibiotics and bacterial resistance in the 21st Century. Perspect Medicin Chem 2014;6:25–64.
DOI:10.4137/PMC.S14459
5. Monisha J, Tenzin T, Naresh A, Blessy BM, Krishnamurthy NB. Toxicity, mechanism and health effects of some heavy metals. Interdiscip Toxicol. 7(2):60–72.
DOI: 10.2478/intox-2014-0009
6. Glenn ST, Nicolette T. New and alternative approaches to tackling antibiotic resistance. F1000Prime Rep. 2013;5:51.
DOI: 10.12703/P5-51.
7. Festus C, Ekennia AC, Collins UI, Okafore SN, Onwudiwe DC., Osowole AA, Oguejiofo TU. Synthesis, characterization, antimicrobial activity and DFT studies of 2-(pyrimidin-2-ylamino)naphthalene-1,4-dione and its Mn(II), Co(II), Ni(II) and Zn(II) complexes. J. of Molecular Structure. 2018;1163:455-464;
https://doi.org/10.1016/j.molstruc.2018.03.025 0022-2860.
8. Graham LP. An introduction to medicinal chemistry 3rd Edition. Oxford University press, UK; 2005.

9. Parveez G, Athar AH. Biological activity studies on metal complexes of macrocyclic Schiff base Ligand: Synthesis and spectroscopic characterization. J. Braz. Chem. Soc. 2015;26(7):1331-1337. doi.org/10.5935/0103-5053.20150099.

10. Samuel T, David KD, Regina A, Isaac T. Spectroscopic characterization, In Vitro cytotoxicity, and antioxidant activity of mixed ligand Palladium(II) Chloride Complexes Bearing Nucleobases. Journal of Inorganic Chemistry; 2014. dx.doi.org/10.1155/2014/586131.

11. Osowole AA, Festus C. Synthesis, spectral magnetic and antibacterial studies of some divalent metal complexes of 3-{[(4,6-dihydroxy pyrimidin-2-yl)Imino]methyl}Napthalen-2-ol. Journal of Chemical, Biological and physical sciences, 2015;6(11):210-219, www.jcbsc.org.

12. Osowole AA, Festus C. Synthesis, characterization and antibacterial activities of some metal(II)complexes of 3-(-1-(2-pyrimidinylimino)methyl-2-napthol. Elixir Appl. Chem. 2013;59: 15843- 15847.

13. Tetteh S, Dodoo DK, Appiah-Opong R, Tuffour I. Spectroscopic characterization, In Vitro cytotoxicity, and antioxidant activity of mixed ligand Palladium(II) chloride complexes bearing nucleobases. J. of Inorg. Chem; 2014. doi.org/10.1155/2014/586131

14. Festus C, Ibeji CU, Okpareke O. Novel 3d divalent metallic complexes of 3-[(2-hydroxy-5-methylphenylimino)-methyl]-napthalen-2-ol: Synthesis, spectral, characterization, antimicrobial and computational studies. Journal of Molecular Structure. 2020'1210:1-13.

15. Zoubi, W.A., Kandil, F. and Chebani, M. K. (2012). Synthesis of macrocyclic Schiff bases based on pyridine-2,6-dicarbohydrazide and their use in metal cations extraction. Organic chemistry Current research. 1(1):1-7

16. Chioma, F, Ozioma AE, Don-Lawson CD. Novel metal2+ complexes of N-(1,4-dihydro-1,4-oxonaphthalen-3-yl) pyrazine-2-carboxamide: Synthesis, structural characterization, magnetic properties and antimicrobial activities. Curr. Res. Chem. 2020;12:1-10

17. Festus C, Jude IA, Collins UI. Ligation Actions of 2-(3-hydroxypyridin-2-ylamino) naphthalen-1,4-dione: Synthesis, characterization, In-vitro antimicrobial screening, and computational studies. Indian J. of Heterocyclic Chemistry, 2010; 31(01):1-13.

18. Valarmathy, G. and Subbalakshmi, R. Synthesis, spectral characterisation, electrochemical, and fluorescence studies of biologically active novel Schiff base complexes derived from E-4-(2-hydroxy-3-methoxybenzlideneamino)-N-(pyrimidin-2-yl) benzenesulfonamide. Turkish Journal of Chemistry 2014;38:521-530

19. Jayabalakrishnan C, Natarajan K. Ruthenium(II) carbonyl complexes with tridentate Schiff bases and their antibacterial activity. Transition Metal Chem. 2002;27(1):75–79

20. Festus C, Anthony CE, Osowole AA, Lukman OO, Damian CO, Oguejiofo TU. Synthesis, experimental and theoretical characterization and antimicrobial studies of some Fe(II), Co(II) and Ni(II) complexes of 2-(4,6-dihydroxypyrimidin-2-ylamino) naphthalene-1,4-dione. Research on Chemical Intermediates 2018b;44(10): 5857-5877
DOI 10.1007/s11164-018-3460-7

21. Kalsi PS. Spectroscopy of organic compounds. 6th Edition. New age International publishers, India 2004;71-7249.

22. Damian CO, Anthony CE, Eric H. Syntheses, characterization, and antimicrobial properties of nickel(II) dithiocarbamate complexes containing NiS4 and NiS2PN moieties, Journal of Coordination Chemistry; 2016.
DOI:10.1080/00958972.2016.1186800

23. Salmon L, Molnar G, Cobo S, Oulié P, Etienne M, Mahfoud T, Demont P, Eguchi A, Watanabe H, Tanaka K, Bousseksou A. Reinvestigation of the spin crossover phenomenon in the ferrous complex [Fe(HB(pz)₃)₂]. New Journal of Chemistry 2009;33(6):1283-1289.
https://doi.org/10.1039/B902811K

24. Festus C, Ekpete OA, Don-Lawson CD. Novel metal2+ complexes of N-(1,4-dihydro-1,4-oxonaphthalen-3-yl) pyrazine-2-carboxamide: Synthesis, structural characterization, magnetic properties and antimicrobial activities. Curr. Res. Chem. 2020;12:1-10.
DOI:10. 3923/crc.2020.1.10

25. Cesar S, Maria P, Cristian T. Biologically active transition metal chelates with a 2-thiophenecarboxaldehyde-derived Schiff base: Synthesis, characterization and

antibacterial properties. Turkish Journal of Chemistry 2008;32:487-493.

26. Salmon L, Molnar G, Cobo S, Oulié P, Etienne M, Mahfoud T, Demont P, Eguchi A, Watanabe H, Tanaka K, Bousseksou A. Reinvestigation of the spin crossover phenomenon in the ferrous complex [Fe(HB(pz)$_3$)$_2$]. New J. of Chemistry. 2009;33(6):1283-1289.

27. Festus C, Ekennia AC, Osowole AA, Okafor SN, Ibeji CU, Onwudiwe DC, Ujam OT. Synthesis, characterization, in-vitro antimicrobial properties, molecular docking and DFT studies of 3-{(E)-[(4,6-dimethylpyrimidin-2-yl)imino]methyl}naphthalen-2-ol and Heteroleptic Mn(II), Co(II), Ni(II) and Zn(II) complexes. Open Chem., 2018;16:184–200.
https://doi.org/10.1515/chem-2018-0020

28. Nogrady T. Medical Chemistry:A biochemistry approach. Oxford University Press, New York; 1988.

29. Rama KRK, Suneetha P, Karigar CS, Manjnath NH, Mahendra KN. Cobalt(II),Ni(II), Cu (II), Zn (II), Cd (II), Hg (II),UO2 (VI) and Th (IV) complexes from

ONNN Schiff base ligand,J. Chilean Chem. Soc. 2008;53:1653-1657.

30. Osowole AA, Fagade OE. "Synthesis, characterization and biopotency of some metal(II) β-ketoiminates and their mixed-ligand complexes," Polish Journal of Chemistry. 2007;81(12): 2039–2048.

31. Thangadurai, TD, Natarajan K. Mixed ligand complexes of ruthenium(II) containing α, β-unsaturated-β-ketoamines and their antibacterial activity. Transition Met. Chem. 2001;26:500-504.

32. Singhal S, Khanna P, Khanna L. Synthesis, DFT studies, molecular docking, antimicrobial screening and UV fluorescence studies on ct-DNA for novel Schiff bases of 2-(1-aminobenzyl) benzimidazole. Heliyon, 2019;5(10):e02596.
DOI: 10.1016/j.heliyon.2019.e02596

33. Bououden W, Benguerba Y. Computational Quantum Chemical Study, Drug-Likeness and In Silico Cytotoxicity Evaluation of Some Steroidal Anti-Inflammatory Drugs. J. Of Drug Delivery And Therapeutics. 2014;10(3-s):68-74.
DOI: 10.22270/jddt.v10i3-s.4165

Peer-review history:
The peer review history for this paper can be accessed here:
https://www.sdiarticle5.com/review-history/76868